Optical loss reduction in high-index-contrast chalcogenide glass waveguides via thermal reflow

Juejun Hu,[1*] Ning-Ning Feng,[1] Nathan Carlie,[2] Laeticia Petit,[2] Anu Agarwal,[1] Kathleen Richardson,[2] and Lionel Kimerling[1]

[1]*Microphotonics Center, Massachusetts Institute of Technology, Cambridge, Massachusetts 02139, USA*
[2]*School of Materials Science and Engineering, COMSET, Clemson University, Clemson, SC 29634, USA*
** hujuejun@mit.edu*

Abstract: A thermal reflow technique is applied to high-index-contrast, sub-micron waveguides in As_2S_3 chalcogenide glass to reduce the sidewall roughness and associated optical scattering loss. We show that the reflow process effectively decreases sidewall roughness of chalcogenide glass waveguides. A kinetic model is presented to quantitatively explain the sidewall roughness evolution during thermal reflow. Further, we develop a technique to calculate waveguide optical loss using the roughness evolution model, and predict the ultimate low loss limit in reflowed high-index-contrast glass waveguides. Up to 50% optical loss reduction after reflow treatment is experimentally observed, and the practical loss limiting factors are discussed.

OCIS codes: (130.2790) Guided waves; (130.3120) Integrated optics devices; (130.3130) Integrated optics materials; (160.2750) Glass and other amorphous materials; (230.7390) Waveguides, planar; (240.5770) Roughness; (290.5880) Scattering, rough surfaces.

References and links

1. A. L. Greer, and N. Mathur, "Materials science: changing face of the chameleon," Nature **437**(7063), 1246–1247 (2005).
2. N. Hô, M. C. Phillips, H. Qiao, P. J. Allen, K. Krishnaswami, B. J. Riley, T. L. Myers, and N. C. Anheier, Jr., "Single-mode low-loss chalcogenide glass waveguides for the mid-infrared," Opt. Lett. **31**(12), 1860–1862 (2006).
3. V. Ta'eed, N. J. Baker, L. Fu, K. Finsterbusch, M. R. Lamont, D. J. Moss, H. C. Nguyen, B. J. Eggleton, D. Y. Choi, S. Madden, and B. Luther-Davies, "Ultrafast all-optical chalcogenide glass photonic circuits," Opt. Express **15**(15), 9205–9221 (2007).
4. J. Hu, N. Carlie, N. N. Feng, L. Petit, A. Agarwal, K. Richardson, and L. Kimerling, "Planar waveguide-coupled, high-index-contrast, high-Q resonators in chalcogenide glass for sensing," Opt. Lett. **33**(21), 2500–2502 (2008).
5. M. Pelusi, V. Ta'eed, M. Lamont, S. Madden, D. Choi, B. Luther-Davies, and B. Eggleton, "Ultra-High Nonlinear As_2S_3 Planar Waveguide for 160-Gb/s Optical Time-Division Demultiplexing by Four-Wave Mixing," IEEE Photon. Technol. Lett. **19**(19), 1496–1498 (2007).
6. T. Barwicz, and H. Haus, "Three-dimensional analysis of scattering losses due to sidewall roughness in microphotonic waveguides," J. Lightwave Technol. **23**(9), 2719–2732 (2005).
7. P. Tien, "Light Waves in Thin Films and Integrated Optics," Appl. Opt. **10**(11), 2395–2413 (1971).
8. J. Hu, V. Tarasov, N. Carlie, N. N. Feng, L. Petit, A. Agarwal, K. Richardson, and L. Kimerling, "Si-CMOS-compatible lift-off fabrication of low-loss planar chalcogenide waveguides," Opt. Express **15**(19), 11798–11807 (2007).
9. S. Dutta, H. Jackson, and J. Boyd, "Reduction of scattering from a glass thin-film optical waveguide by CO_2 laser annealing," Appl. Phys. Lett. **37**(6), 512–514 (1980).
10. R. Syms, and A. Holmes, "Reflow and Burial of Channel Waveguides Formed in Sol-Gel Glass on Si Substrates," IEEE Photon. Technol. Lett. **5**(9), 1077–1079 (1993).
11. S. Ramachandran, and S. Bishop, "Low loss photoinduced waveguides in rapid thermally annealed films of chalcogenide glasses," Appl. Phys. Lett. **74**(1), 13–15 (1999).
12. S. Ramachandran, and S. Bishop, "Photoinduced integrated-optic devices in rapid thermally annealed chalcogenide glasses," IEEE J. Sel. Top. Quantum Electron. **11**(1), 260–270 (2005).
13. D. Marcuse, "Radiation Losses of Dielectric Waveguides in Terms of the Power Spectrum of the Wall Distortion Function," Bell Syst. Tech. J. **48**, 3233 (1969).
14. S. Surińach, E. Illekova, G. Zhang, M. Poulain, and M. Baró, "Optical fiber drawing temperature of fluorogallate glasses," J. Mater. Res. **11**(10), 2633–2640 (1996).

#118791 - $15.00 USD Received 20 Oct 2009; revised 23 Dec 2009; accepted 28 Dec 2009; published 12 Jan 2010

15. http://www.amorphousmaterials.com/IR%20Fibers.htm
16. P. Roberts, F. Couny, H. Sabert, B. Mangan, D. Williams, L. Farr, M. Mason, A. Tomlinson, T. Birks, J. Knight, and P. St J Russell, "Ultimate low loss of hollow-core photonic crystal fibres," Opt. Express **13**(1), 236–244 (2005).
17. J. Lacey, and F. Payne, "Radiation loss from planar waveguides with random wall imperfections," IEE Proc. J. **137**, 282–288 (1990).
18. W. Li, S. Seal, C. Rivero, C. Lopez, K. Richardson, A. Pope, A. Schulte, S. Myneni, H. Jain, K. Antoine, and A. Miller, "Role of S/Se ratio in chemical bonding of As-S-Se glasses investigated by Raman, x-ray photoelectron, and extended x-ray absorption fine structure spectroscopies," J. Appl. Phys. **98**(5), 053503 (2005).
19. J. Hu, V. Tarasov, A. Agarwal, L. Kimerling, N. Carlie, L. Petit, and K. Richardson, "Fabrication and testing of planar chalcogenide waveguide integrated microfluidic sensor," Opt. Express **15**(5), 2307–2314 (2007).
20. Patterned As_2S_3 films are highly susceptible to surface oxidation and thus need to be protected by polymer coatings (e.g. SU8) for long-term stability. Our XPS study has confirmed the presence of surface As_2O_x oxides on as-patterned As_2S_3 waveguides exposed in ambient air for just a few hours.
21. R. Wang, S. Madden, C. Zha, A. Rode, and B. Luther-Davies, "Annealing induced phase transformation in amorphous As_2S_3 films," J. Appl. Phys. **100**(6), 063524 (2006).
22. N.-N. Feng, G.-R. Zhou, C. Xu, and W.-P. Huang, "Computation of full-vector modes for bending waveguide using cylindrical perfectly matched layers," J. Lightwave Technol. **20**(11), 1976–1980 (2002).

1. Introduction

High index contrast (HIC) waveguides and photonic devices offer key competitive advantages over low index contrast (LIC) waveguides; these advantages include a small device footprint suitable for high density integration, and strong optical confinement with enhanced linear and nonlinear optical effects. In particular, chalcogenide glasses (ChG's) have recently emerged as a promising material candidate for HIC photonic devices, featuring almost an unlimited capacity for composition and property tailoring [1], ultra-wide infrared transparency[2], and high Kerr nonlinearity accompanied with low two photon absorption (TPA) [3]. An array of technical applications that leverage the unique properties of chalcogenide glasses as well as the HIC integration benefits, including biochemical sensing [4] and all-optical signal processing [5], have been demonstrated. However, HIC waveguides typically suffer much higher propagation losses than their LIC counterparts, mainly due to increased optical scattering from sidewall roughness, which scales with the square of refractive index contrast [6, 7]. Our previous study has also confirmed that optical scattering arising from sidewall roughness is the dominant source of optical loss in HIC chalcogenide strip waveguides [8]. Such high scattering loss limits the ultimate performance improvement possible in chalcogenide glass HIC photonic devices.

In this paper, we present thermal reflow as an effective approach for sidewall roughness and optical loss reduction in HIC chalcogenide waveguide devices. Analogous to a fiber drawing process, the action of surface tension leads to smoothing of roughness and thus creation of negligible scattering loss. Thermal reflow has been shown to effectively decrease optical loss in silica glass [9, 10]. It has also been observed that surface roughness of as-deposited chalcogenide glass films is decreased after rapid thermal annealing [11, 12]. Here we demonstrate the first application of a reflow technique to optical loss reduction in chalcogenide glass waveguides. Compared to the silica glass reflow process, chalcogenide glass reflow does not require thermal processing at elevated temperatures given the lower softening temperature of chalcogenides. Such a tolerant thermal budget is compatible with CMOS backend processes and imposes minimal adverse effect on other on-chip devices, an advantage for electronic and photonic integration.

2. Kinetic theory of roughness vvolution during reflow

Sidewall roughness reduction during reflow is driven by surface tension of glass towards minimization of surface energy, and therefore the kinetics of this process is determined by the interaction between the surface tension force and glass viscosity. We first consider a glass surface perpendicular to the y-axis and featured by roughness described by a 1-d sinusoidal wave with a characteristic wavelength L as is shown in Fig. 1(a):

#118791 - $15.00 USD Received 20 Oct 2009; revised 23 Dec 2009; accepted 28 Dec 2009; published 12 Jan 2010

$$H'(z) = H_L \sin(\frac{2\pi}{L} z) \tag{1}$$

where H is the y-coordinate of the glass surface, and H_L gives the roughness amplitude.

Since glass typically exhibits relatively high viscosity, we can assume Newtonian behavior of glass with low Reynold number. Further, gravity is much smaller compared to surface tension and thus can be neglected. In this case, the reflow process is governed by the following equations:

$$\text{Continuity equation:} \quad \frac{\partial v_z}{\partial z} + \frac{\partial v_x}{\partial x} = 0 \tag{2}$$

$$\text{Force equilibrium:} \quad -\mu \frac{\partial^2 v_x}{\partial z^2} = \frac{\partial p}{\partial x} \tag{3}$$

$$\mu \frac{\partial^2 v_z}{\partial x^2} = \frac{\partial p}{\partial z} \tag{4}$$

Here Eq. (2) imposes the mass conservation constraint on viscous flow in the glass, where v_x and v_z are both functions of x and z spatial coordinates, denoting the flow velocity in the glass. Since v_x and v_z are typically very small given the short length scale under investigation, a quasi-static approximation applies and the force equilibrium conditions Eq. (3) and (4) hold, where μ is the glass kinetic viscosity and p represents the internal pressure in the glass due to surface tension. In addition, the internal pressure on the glass surface arising from surface tension given by:

$$p_{surface} = -T \frac{\partial^2 H'}{\partial z^2} = \frac{4\pi^2}{L^2} T H_L \sin(\frac{2\pi}{L} z) \tag{5}$$

specifies the boundary condition of this 2-d problem, where T is the surface tension (N/m) of glass at the reflow temperature.

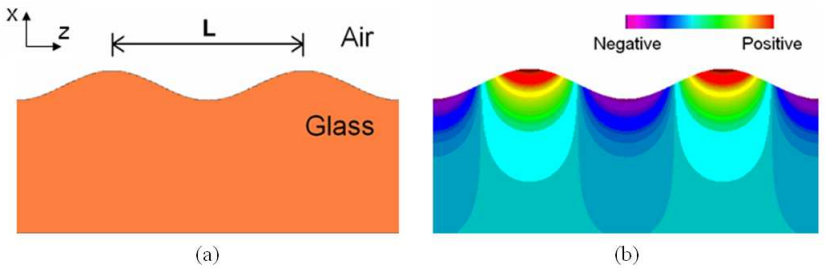

Fig. 1. (a) Schematic illustration of a glass surface with sinusoidal roughness characterized by a spatial period L; (b) calculated internal pressure due to surface tension in glass with a rough surface.

Due to the phase matching constraint, the roughness wavelengths contributing to scattering loss lie in a range given by [13]:

$$\beta - \frac{2\pi}{\lambda_{clad}} < L < \beta + \frac{2\pi}{\lambda_{clad}} \tag{6}$$

where β is the propagation constant in the waveguide, and λ_{clad} is the wavelength in the cladding. For HIC waveguides, typically this represents spatial periods between 100 nm to a few microns at telecommunication wavelengths. Meanwhile, waveguide sidewall RMS roughness usually ranges from a few to a few tenths of nanometers. Consequently, with the

#118791 - $15.00 USD Received 20 Oct 2009; revised 23 Dec 2009; accepted 28 Dec 2009; published 12 Jan 2010

valid approximation H' << L, Eq. (2), (3) and (4) have a closed form solution represented by the following set of equations:

$$v_z = \frac{2\pi}{L}\frac{TH_L}{\mu} \times \exp(-\frac{2\pi}{L}x) \times \cos(\frac{2\pi}{L}z) \tag{7}$$

$$v_x = -\frac{2\pi}{L}\frac{TH_L}{\mu} \times \exp(-\frac{2\pi}{L}x) \times \sin(\frac{2\pi}{L}z) \tag{8}$$

$$p = \frac{4\pi^2}{L^2}TH_L \times \exp(-\frac{2\pi}{L}x) \times \sin(\frac{2\pi}{L}z) \tag{9}$$

A color contour map in Fig. 1(b) illustrates the internal pressure p distribution in the glass according to Eq. (9). Decay rate of roughness amplitude H_L is thus given by v_x at the glass surface, which yields an exponential decay with a time constant t:

$$t = \frac{L\mu}{2\pi T} \tag{10}$$

This time constant provides an estimation on the reflow time duration necessary for significant roughness reduction to take place. For example, assuming the reflow process is performed within the fiber drawing viscosity window (10^3 to 10^6 Pa·s [14]), the time it takes for a 10-fold decrease of roughness with a characteristic wavelength of 1 μm is approximately 10^{-3} to 0.1 s. Such a time scale is much shorter compared to the dwelling time of glass preform in a fiber drawing furnace. We note that state-of-the-art chalcogenide glass fibers can achieve the very low optical loss (~dB/m) near 1550 nm wavelength [15], which indicates that precipitation of crystallites leading to optical scattering loss can be suppressed in the fiber drawing thermal process. Thus this analogy suggests that it is possible to achieve low loss chalcogenide waveguides via thermal reflow without compromising the glass material quality, given the short reflow time required and hence low crystallization tendency.

In general, since the boundary condition Eq. (5) is linear, the analytical solution for a surface with a random roughness distribution can be obtained through simple harmonic analysis. An arbitrary 1-d roughness distribution along the z-axis between $[-z_0, z_0]$ can be described using a function H(z). The time evolution of H(z, t) can then be characterized by the amplitude decay of its Fourier components:

$$h_k(t=0) = \frac{1}{2z_0}\int_{-z_0}^{z_0} H(z, t=0) \cdot \exp(-i\frac{\pi k}{z_0}z)dz \tag{11}$$

$$H(z,t) = \sum_{k=-\infty}^{+\infty} h_k(t=0) \cdot \exp(-i\frac{\pi k}{z_0}z - \frac{\pi T k}{z_0 \mu}t) \tag{12}$$

In an ideal viscous glass melt free of crystallization, this evolution trend continues until an ultimate roughness limit is reached. This ultimate roughness limit that can possibly be achieved via thermal reflow is set forth by the equi-partition of energy in surface capillary wave modes at glass transition [16].

The kinetic theory also establishes the quantitative relation between roughness evolution during reflow and optical waveguide loss reduction. For any given sidewall roughness distribution described by a roughness autocorrelation function R(z'), the kinetic analysis above provides a method to quantitatively predict the time evolution of R(z') during reflow. As an example, we assume the starting roughness in on the top surface of a slab waveguide can be described by an exponential model [17], which yields a roughness autocorrelation function in the form:

#118791 - $15.00 USD Received 20 Oct 2009; revised 23 Dec 2009; accepted 28 Dec 2009; published 12 Jan 2010

$$R(z') = \sigma^2 \cdot \exp(-\frac{|z'|}{L_c}) \qquad (13)$$

where L_c denotes the correlation length and σ^2 is the roughness variance. Figure 2a compares autocorrelation functions before and after reflow treatment, as is predicted by the kinetic reflow model (see Appendix for details). Notably R(z') is significantly modified after reflow. If we still use an exponential model as an approximation, the reflow treatment results in reduction of roughness variance and increased correlation length, factors that need to be taken into account when making waveguide loss predictions. According to the Payne-Lacey model [15], the scattering loss in a slab waveguide with a rough surface can be calculated from the autocorrelation function:

$$\alpha_s = \varphi^2(\frac{d}{2}) \cdot (n_1^2 - n_2^2) \cdot \frac{k_0^3}{8\pi \cdot n_1} \cdot \int_0^{\pi} \overline{R}(\beta - n_2 k_0 \cos\theta) d\theta \qquad (12)$$

where n_1 and n_2 are the core and cladding refractive indices, respectively, k_0 is the free space wave vector, d represents the waveguide thickness, β denotes the waveguide modal propagation constant, $\phi(d/2)$ is the modal field amplitude at the waveguide surface and is normalized so that:

$$\int_{-\infty}^{\infty} \varphi(x) dx = 1 \qquad (13)$$

and $\overline{R}$ is the roughness spectral density, which is given by the Fourier transform of the autocorrelation function:

$$\overline{R}(\xi) = \int_{-\infty}^{\infty} R(z') \cdot \exp(i\xi \cdot z') dz' \qquad (14)$$

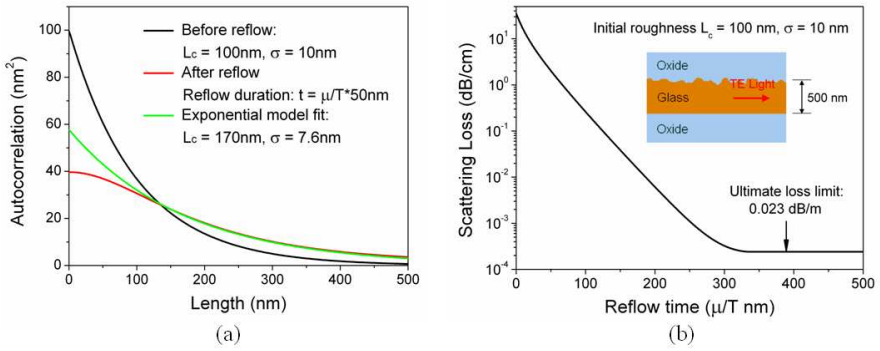

Fig. 2. (a) Autocorrelation functions of waveguide sidewall roughness before and after reflow treatment predicted by the kinetic analysis: the black curve is the initial roughness in as-patterned waveguide (assume a correlation length L_c = 100 nm and roughness variance σ = 10 nm), the red curve corresponds to roughness after reflow treatment for a duration t_0 = μ/T·50 nm, and the green curve is the numerical fit of the roughness autocorrelation after reflow using an exponential model; (b) scattering loss evolution as a function of reflow time (given in μ/T·nm) for TE polarization light in a 500 nm thick As_2S_3 slab waveguide (index contrast Δn = 0.92) with a rough top surface, calculated using the Payne-Lacey model and the autocorrelation functions predicted by the reflow kinetic theory. The ultimate loss is limited by equi-partition of energy in surface capillary wave modes. The inset gives the assumed initial roughness parameters and the slab waveguide configuration.

Figure 2(b) plots the calculated TE polarization scattering loss in an As_2S_3 slab waveguide embedded in oxide claddings as a function of reflow time, assuming that no material degradation such as crystallization occurs in the process. The faster decay in the initial stage is a consequence of rapidly vanishing roughness components with short spatial wavelengths.

#118791 - $15.00 USD Received 20 Oct 2009; revised 23 Dec 2009; accepted 28 Dec 2009; published 12 Jan 2010

The ultimate low loss bounded by frozen-in surface capillary wave is represented by the horizontal line at long time limit.

More rigorous scattering loss models [6] may be employed to quantitatively evaluate loss reduction after thermal reflow in waveguides with more complex geometries, such as strip waveguides and rib waveguides. Detailed discussions, however, are not within the scope of this paper due to the complicated mathematical treatment involved.

3. Experimental

Strip waveguides with a width of 800 nm and a height of 400 nm in thermally evaporated As_2S_3 films (n = 2.37 at 1550 nm) are patterned via lift-off on 3 μm thermal oxide coated Si wafers. The entire patterning process is carried out on a 500 nm CMOS line [8]. The bulk glass preparation and film deposition process are described in detail elsewhere [18, 19]. Thermal reflow of the as-patterned waveguide devices has been carried out at different temperatures (± 5 °C) on a pre-heated hotplate in a nitrogen filled glove box (oxygen and water vapor impurity < 10 ppm). Given the relatively short reflow time scale as is shown in the theoretical analysis section, we choose to vary the reflow temperature and fix the reflow time to 15 s. Since viscous flow of glass is often a thermally activated process and the glass viscosity exhibits an Arrhenius-type temperature dependence, varying reflow temperature effectively changes the time constant in Eq. (10). After heat treatment, the samples are immediately transferred onto an aluminum heat sink held at room temperature to minimize dwelling time at intermediate temperatures. The time to reach thermal equilibrium in the rapid annealing and quenching process is estimated to be < 3 s via a simple multi-layer heat transfer simulation.

A Digital Instruments Nanoscope IIIa Atomic Force Microscope (AFM) is used to measure the roughness of as-patterned and reflowed unclad As_2S_3 waveguides. AFM scans are performed parallel to the direction of the waveguides using the tapping mode. Measurements are performed at different locations across the substrate and the resulting roughness data are averaged to minimize statistical error. The data obtained is analyzed using the Digital Instruments Nanoscope Software.

Before characterizing optical properties, the as-patterned and reflowed devices were spin coated with a 3 μm thick layer of SU8 polymer to prevent surface oxidation. The devices are subsequently annealed at 140°C for 3 h to stabilize the glass structure. Cavity quality factors (Q-factors) of racetrack micro-resonators with a bending radius of 50 μm comprising of strip As_2S_3 waveguides are measured using a fiber end-fire technique. The corresponding optical loss in the waveguides is calculated via:

$$Q_{cr} = \frac{\lambda_0}{(\Delta\lambda)_{3dB}} = \frac{\pi n_g}{\alpha\lambda_0} \tag{17}$$

where Q_{cr} is the loaded cavity Q-factor at critical coupling, λ_0 denotes the resonant wavelength, n_g stands for the waveguide group index, and α represents the linear waveguide optical loss coefficient in cm^{-1}. Multiple (6 to 12) tests are performed on different resonator devices and the results are averaged to avoid statistical error in the loss measurement. Since our measurement gives a low material absorption of < 2 dB/cm in SU8 polymer, we can state that contributions to the waveguide loss figures measured from Eq. (17) come from surface roughness scattering and radiative loss due to waveguide bending and substrate leakage.

4. Results and discussion

Figure 3 shows the surface morphology of chalcogenide glass waveguides before and after reflow at two different temperatures (> 50 °C above glass transition) for 15 s. It is clear that the sidewall roughness is significantly reduced after reflow, and at the same time the waveguide cross-sectional geometry is also modified towards a dome shape due to surface tension. The origin of such sidewall roughness in the chalcogenide waveguides is attributed to the edge roughness of photoresist mask prior to lift-off as is shown in Fig. 4(a). Further

#118791 - $15.00 USD Received 20 Oct 2009; revised 23 Dec 2009; accepted 28 Dec 2009; published 12 Jan 2010

optimization of the lift-off process including fine-tuning the exposure dose and applying an anti-reflection coating during lithography will help reduce the roughness. Sidewall roughness amplitude as functions of different spatial periods is plotted in Fig. 4(b). Roughness with smaller spatial wavelength exhibits more significant amplitude reduction, which agrees with the kinetic theory analysis. Quantitatively, the olive curve in Fig. 4(b) gives the roughness amplitude after 15 s reflow at 220 °C predicted by the reflow kinetic theory based on as-patterned roughness values. The deviation from theoretical predictions at short spatial wavelengths suggests the presence of limiting mechanisms to roughness reduction. Such an observation could be attributed to the local surface oxidation of As_2S_3 glass and the formation of As_2O_x nanocrystals and is not intrinsic to the reflow process [20].

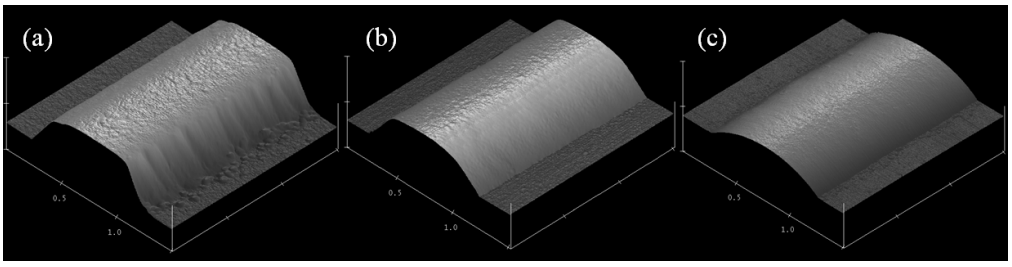

Fig. 3. Surface morphology of As_2S_3 chalcogenide waveguides measured by AFM: (a) as-patterned; (b) reflowed at 230 °C for 15 s exhibiting reduced sidewall roughness; and (c) reflowed at 245 °C for 15 s showing significant cross-sectional geometry modification.

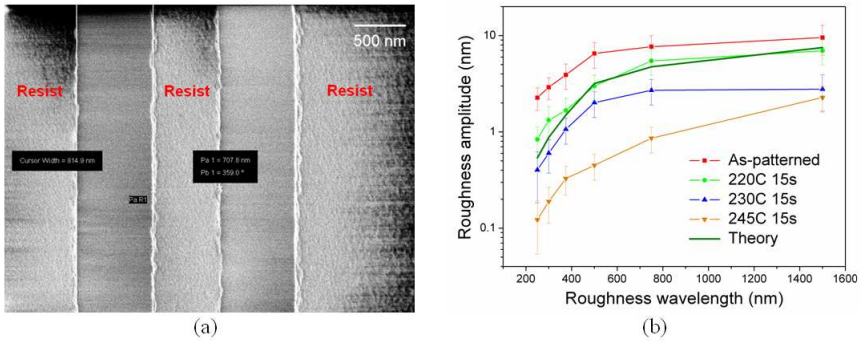

Fig. 4. (a). A top-view SEM micrograph showing the presence of edge roughness on photo resist mask prior to lift-off; (b). waveguide roughness amplitude as a function of roughness wavelength for different reflow temperatures: the olive curve is the roughness amplitude after 15 s reflow at 220 °C predicted by the reflow kinetic theory based on as-patterned roughness values.

Figure 5 plots the transmission loss in As_2S_3 waveguides after reflow treatment at different temperatures. The optical loss decrease after 15 s reflow at 220 °C and 230 °C is consistent with the trend of sidewall roughness smoothing. In addition, waveguide loss due to As_2S_3 material absorption is estimated to be < 0.6 dB/cm based on our loss measurement results in As_2S_3 microdisk resonators [4]. Therefore the observed loss decrease can be attributed to scattering loss reduction due to reflow. However, despite the continuing trend of roughness reduction at increased reflow temperature, optical loss in As_2S_3 waveguides sharply increases to ~(18 ± 5) dB/cm after 15 s reflow at 245 °C. Composition analysis performed on blanket As_2S_3 films reflowed at 245 °C reveals that the composition change after the thermal treatment is within the detection limit of electron wavelength dispersive spectroscopy (WDS), which is estimated to be ~2% atomic ratio. Therefore, parasitic optical attenuation due to sulfur loss (vaporization), which often occurs when annealing As_2S_3, is insignificant in our case. Consequently, here we investigate two possible mechanisms for the loss increase: 1) formation of crystal precipitates from As_2S_3 glass and the ensuing optical scattering; and/or 2)

#118791 - $15.00 USD Received 20 Oct 2009; revised 23 Dec 2009; accepted 28 Dec 2009; published 12 Jan 2010

radiative loss increase due to waveguide cross-section modification. In investigating the first hypothesis of nanocrystallite scattering being the major loss-contributor: previous work has shown that annealing As_2S_3 films leads to partial crystallization of the glass, a process that is accelerated at elevated temperatures [21]. Since no distinctive sharp crystalline peak is resolved in X-ray diffraction (XRD) analysis of blanket As_2S_3 films reflowed at 245 °C, we exclude the presence of large-size, ordered crystalline precipitates throughout the bulk structure of the waveguide. As a simple estimation, if we assume the scattering centers are uniformly distributed in As_2S_3 glass, the resulting waveguide loss due to Rayleigh scattering is given by:

$$\alpha_R = 24\pi^3 N_p V^2 \left(\frac{n^2 - n_0^2}{n^2 + 2n_0^2}\right)^2 \cdot \left(\frac{n_0}{\lambda}\right)^4 \cdot \Gamma \qquad (18)$$

where N_p is the volume density of scattering centers, V is the volume of crystallites, λ gives the free-space wavelength, Γ is the waveguide confinement factor, and n = 2.74 and n_0 = 2.37 represent the refractive indices of crystallites (taken as the ensemble averaged index of randomly oriented As_2S_3 orpiment crystalline particles) and As_2S_3 glass matrix at 1550 nm, respectively. Equation (18) is originally derived for scattering events in free space, and thus it actually overestimates the scattering loss in a waveguide since the presence of optical confinement modifies the dipole radiation pattern and reduces radiation efficiency. Assuming an average crystallite size of 10 nm, Eq. (18) gives a scattering center volume fraction exceeding unity, a physically impractical result. Therefore, the high loss of waveguides reflowed at 245 °C cannot be solely explained by scattering due to nano-crystallization.

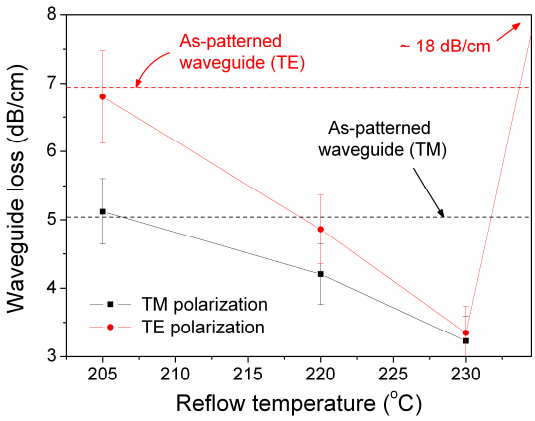

Fig. 5. Measured As_2S_3 waveguide loss (± 10%) after 15 s reflow treatment at different temperatures. The optical loss values in as-patterned As_2S_3 waveguides are represented by the two horizontal lines.

Alternatively, while investigating the second hypothesis of radiative loss being the major loss-contributor, we notice that the waveguide height decreases from 400 nm to ~200 nm after a reflow treatment at 245 °C, which may be attributed to the partial evaporation of As_2S_3 glass. Such film thickness decrease due to partial evaporation also visually manifests as slight color change in blanket As_2S_3 glass films reflowed at 245 °C. Notably, thermogravimetry analysis (TGA) measurement performed at the same temperature using As_2S_3 powders manually crushed from bulk glasses gives negligible fractional weight loss (< 5%). Therefore, we conclude that the increased surface to volume ratio in patterned glass thin films gives rise to enhanced vaporization.

To quantitatively evaluate the optical radiative loss increase due to such waveguide cross-section modification, we perform waveguide modal simulations. Experimentally measured waveguide cross-sectional geometry is used as the input for finite difference (FD) modal simulations. The resulting waveguide bending loss and substrate leakage loss are calculated

#118791 - $15.00 USD Received 20 Oct 2009; revised 23 Dec 2009; accepted 28 Dec 2009; published 12 Jan 2010

by full-vectorial bending mode solver incorporating cylindrical perfectly matching boundary layers (CPML) in the FD simulations [22]. Modal mismatch loss between the straight and curved sections in a racetrack resonator is simulated using a mode-matching technique and is listed in the table as a distributed loss figure in dB/cm. The simulated loss values are tabulated in Table 1. Notably, the waveguide reflowed at 245 °C becomes highly susceptible to the three radiative loss mechanisms, whose simulated loss figures also exhibit strong dependence on the actual thickness value. In addition, we observe monotonically increasing optical loss at longer wavelengths in waveguides reflowed at 245 °C as is shown in Fig. 6, a phenomenon which is expected if radiative loss is the major loss contributor but inconsistent with the crystal precipitate scattering hypothesis. For practical applications, the radiative loss, proven here as the primary source of loss in our lift-off patterned waveguides, may be further reduced by appropriate waveguide engineering or application of a conformal protective coating, leading to a larger optical loss reduction via thermal reflow.

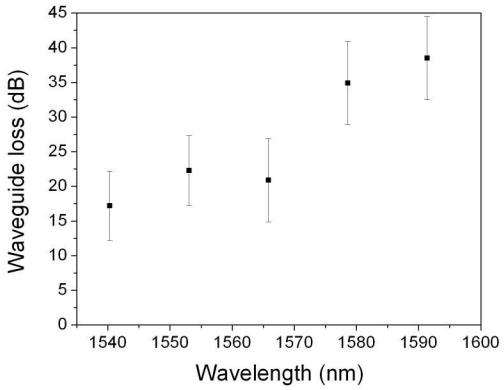

Fig. 6. Measured As_2S_3 waveguide loss after 15 s reflow at 245 °C: the increased optical loss at longer wavelength is characteristic of radiative loss mechanisms but is not expected by the crystalline precipitation scattering hypothesis.

5. Summary and conclusion

We have demonstrated optical loss reduction in HIC As_2S_3 chalcogenide glass waveguide using a thermal reflow treatment. The surface roughness and waveguide optical loss reduction during the reflow process can be quantitatively explained by a kinetic theory. Up to 50% optical loss decrease is experimentally achieved after reflow. Based on material characterization and waveguide modal analysis, the sharp optical loss increase in As_2S_3 waveguides reflowed at higher temperature (245 °C) is attributed to partial evaporation of As_2S_3 glass and the resulting radiative loss. This novel thermal reflow approach opens up new avenues for low-loss photonic applications using chalcogenide glass materials.

Table 1. Simulated optical radiative loss at 1550 nm wavelength in as-patterned and reflowed As_2S_3 waveguides

Type of loss	Polarization	As-patterned waveguide	Waveguide reflowed at 230 °C for 15 s	Waveguide reflowed at 245 °C for 15 s
Bending loss (dB/cm)	TE	8.6×10^{-10}	2.9×10^{-9}	4.8
	TM	7.6×10^{-5}	5.9×10^{-2}	Cut off
Substrate leakage loss (dB/cm)	TE	1.7×10^{-10}	2.7×10^{-9}	3.5×10^{-3}
	TM	1.6×10^{-7}	9.2×10^{-3}	Cut off
Modal mismatch 1oss (dB/cm)	TE	4.0×10^{-3}	4.8×10^{-3}	8.5
	TM	1.0×10^{-2}	2.8×10^{-2}	Cut off

#118791 - $15.00 USD Received 20 Oct 2009; revised 23 Dec 2009; accepted 28 Dec 2009; published 12 Jan 2010

Appendix: calculation of autocorrelation function evolution during reflow

In general the 1-d sidewall roughness distribution function $\tilde{H}(z)$ is defined between $[-\infty, \infty]$, and the roughness autocorrelation function R(z') is defined in terms of ensemble average. To calculate the ensemble average, we instead consider a roughness distribution H(z) defined in the finite domain $[-z_0, z_0]$. By applying a periodic boundary condition, H(z) can be extended for any real z value. In this case we have:

$$R(z') = \left\langle \tilde{H}(z) \cdot \tilde{H}(z+z') \right\rangle \xleftrightarrow{z' << z_0} \frac{1}{2z_0} \int_{-z_0}^{z_0} H(z) \cdot H(z+z') dz \qquad (19)$$

where the brackets represent the ensemble average (expected values). When $z' << z_0$, R(z') can approximated by the right-hand-side integration form using the periodically extended function H(z). According to the Weiner-Kintchine theorem:

$$\sum_{k=-\infty}^{\infty} |h_k|^2 \cdot \exp(-\frac{i \cdot \pi \cdot k}{z_0} z') = \frac{1}{2z_0} \int_{-z_0}^{z_0} H(z) \cdot H(z+z') dz \qquad (20)$$

For any given initial autocorrelation function R(z'), its corresponding Fourier series coefficient $|h_k|^2$ (t = 0) can be calculated using Eq. (20). Additionally, the time evolution of $|h_k|^2$ (t) is quantitatively predicted by Eq. (11). Therefore R(z', t) can be derived by applying an inverse Fourier transformation to $|h_k|^2$ (t).

Acknowledgements

This work is sponsored under the Defense Advanced Research Projects Agency's ULLW program. The program is executed by the Microsystems Technology Office (MTO) under Award No. 017535-001, ARO Award No. W911NF-09-1-0411, Program Code: A.07. Partial funding support is provided by the Department of Energy under award number DE-SC52-06NA27341. The authors also acknowledge the Center for Materials Science and Engineering at MIT and the Microsystems Technology Laboratories at MIT for characterization and fabrication facilities.

#118791 - $15.00 USD Received 20 Oct 2009; revised 23 Dec 2009; accepted 28 Dec 2009; published 12 Jan 2010